


 Cite this: *Nanoscale*, 2025, **17**, 22914

Cytochrome *c* adsorption on carboxylated surfaces: charge regulation and protein orientation modulated by surface curvature

 Sebastian M. Zangoni, †^{a,b} Yamila A. Perez Sirkin, *†^{a,b}
 Estefania Gonzalez Solveyra ^{c,d} and Maria Ana Castro *^{a,b}

Precise control over protein–surface interactions is crucial for designing functional hybrid nanomaterials. Nanoscale curvature, especially in polymer-coated particles, can significantly modulate polymer behavior and surface properties, altering how proteins adsorb. Previous studies on cytochrome *c* (cytC) adsorption have focused on planar surfaces and have largely overlooked how nanoscale curvature, charge-regulating polymer brushes, and protein's orientation and redox state act together. We quantify how curvature, pH, and salt concentration regulate cytC adsorption to carboxyl-terminated polymer brushes using molecular theory with coarse-grained models on planar and nanoparticle surfaces. Results show cytC's oxidation state dictates its orientation but not adsorption energy. Charge regulation is pivotal: as the protein approaches the brush, lysine and histidine residues protonate whereas the polymer deprotonates, a cooperative response controlled by pH and ionic strength. Curvature shifts the equilibrium protein–surface distance by a few nanometers and modulates the orientation of the heme group. These findings not only explain previous observations of enhanced electron transfer in curved nanostructures but also provide practical guidelines and a mechanistic framework for leveraging curvature as a tool in the rational design of nanoparticle-based electrodes and catalysts.

 Received 31st May 2025,
 Accepted 15th September 2025

DOI: 10.1039/d5nr02326b

rsc.li/nanoscale

Introduction

Advances in nanomaterial fabrication have created a wide range of hybrid systems that combine inorganic components with polymers and biomolecules. These nanostructures support applications in electronics, energy, environmental remediation, and biomedicine.^{1,2} Protein adsorption is a constant challenge because, when it is controlled, it can improve the performance of biosensors,³ drug-delivery carriers,⁴ and catalysts,^{5,6} but when it is unchecked, it turns into biofouling and has the opposite effect.^{7,8}

While considerable research has focused on protein adsorption on planar, polymer-modified surfaces, much less is understood about their behavior on surfaces with nanoscale curvature, such as nanoparticles (NPs) and nanofibers.⁹ Many NPs are coated with polymer brushes to improve stability and biocompatibility. Curvature alters the conformational freedom and packing density of the grafted chains. Experimental and theoretical studies show that their degree of ionization depends on pH, salt concentration, and curvature; in fact, when the surface is highly curved, the extra free volume can shift the apparent pK_a by up to two pH units.^{10,11}

This curvature-induced charge regulation strongly influences how incoming proteins sense and respond to the local electric field.¹² Moreover, nanoscale curvature has also been shown to modulate protein orientation on surfaces, from gradual alignment shifts to pH-dependent reorientation.^{13,14} A molecular level understanding of these effects is therefore essential for designing nanomaterials with tailored protein interactions. These curvature-induced effects become increasingly important in systems where the dimensions approach the size of the biomolecule itself. Our study addresses this need by focusing on the adsorption of cytochrome *c* (cytC) onto polymer-modified surfaces with varying curvature. CytC is a key electron transfer (ET) protein in mitochondrial respiration. Its compact, relatively rigid structure,

^aUniversidad de Buenos Aires, Facultad de Ciencias Exactas y Naturales, Departamento de Química Inorgánica Analítica y Química Física, Ciudad Autónoma de Buenos Aires, C1428, Argentina. E-mail: yperezsirkin@qi.fcen.uba.ar, macastro@qi.fcen.uba.ar

^bCONICET-Universidad de Buenos Aires, Instituto de Química de los Materiales, Ambiente y Energía (INQUIMAE), Ciudad Autónoma de Buenos Aires, C1428, Argentina

^cInstituto de Nanosistemas, Escuela de Bio y Nanotecnología, Universidad Nacional de San Martín, Av. 25 de mayo 1169, C1650 Buenos Aires, Argentina

^dConsejo Nacional de Investigaciones Científicas y Técnicas (CONICET), Godoy Cruz 2290, C1414 Ciudad Autónoma de Buenos Aires, Argentina

†These authors contributed equally to this work.

well-characterized redox properties, and extensive experimental and computational literature make it a prime model for studying protein–surface interactions,^{15–18} even within rigid-body approximations.¹⁹ Moreover, clarifying how cytC adsorbs is directly relevant for the design of functional biointerfaces, electrochemical sensors and biocatalytic systems.²⁰ On planar carboxylated self-assembled monolayers (SAMs), the heterogeneous ET rate drops sharply when the protein is rotated.^{21,22} Molecular simulations show that orientation controls ET by modulating electronic coupling and the local dielectric environment,²³ while classic ET theory predicts an exponential dependence on distance.²⁴ Solution conditions such as pH and ionic strength can also switch adsorption on and off.²⁰ Nonetheless, most detailed studies still focus on planar surfaces. Experiments on gold nano-stars, whose spikes are only a few nanometers in radius, report that the ET reaction is favored upon cytC adsorption,²⁵ but the molecular explanation remains open.

While previous studies have examined the adsorption of cytC on planar surfaces, they offer little insight into how nano-scale curvature reshapes this process, especially once charge-regulating polymer brushes and long-range electrostatic interactions are taken into account. As mentioned above, the degree of ionization of such brushes can shift by up to two pH units on highly curved substrates, and proteins themselves adjust their protonation states as they approach a charged interface. How these two forms of charge regulation combine to influence the distance and orientation adopted by cytC, variables that ultimately control electron transfer, remains unresolved. CytC's multiple oxidation states add yet another layer of complexity, as redox transitions redistribute charge and modulate adsorption energetics. Bridging these gaps is essential for building a predictive picture of protein behaviour at nanoparticle surfaces and, in turn, for the rational design of biointerfaces with tailored properties.

Our study addresses this need by using a molecular theory framework with a coarse-grained representation of cytC and polymer brushes to systematically probe the coupled effects of curvature, brush ionization and oxidation state on cytC adsorption. After outlining the theoretical formalism and model parameters, we benchmark the approach on planar carboxylated layers and then extend it to curved interfaces of decreasing radius. We examine how curvature, pH, salt concentration, and redox state shape the adsorption free-energy landscape, charge regulation, and preferred orientation of the protein. Finally, we discuss how the observed trends in curvature-dependent charge regulation and protein orientation provide a mechanistic basis for the rational design of bioelectrodes and other nano-bio interfaces, highlighting curvature as a fundamental design parameter.

Methods

Theoretical framework

In this study, we investigate the effect of the orientation of cytC on its adsorption onto a planar surface or a nanoparticle modified with a polymer brush. Fig. 1A shows a schematic representation of the modeled system.

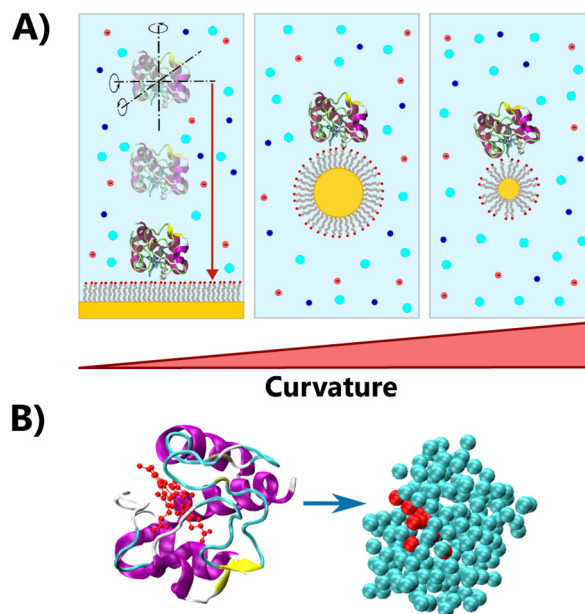


Fig. 1 (A) Schematic representation of the modeled system. A planar or curved surface corresponding to a plane or a nanoparticle of variable radius is coated with a polymeric electrostatic brush (in gray), surrounded by a reservoir of ions (in red and blue) and solvent molecules (in cyan). In each case, a single protein at different distances to the surface is considered. (B) The coarse grained model of the proteins is constructed from the full atom structure obtained from the Protein Data Bank.²⁶

representation of the systems under study. To properly describe them, we employed a molecular theory (MOLT) that explicitly takes into account structural details of the system, the conformational degrees of freedom of the macromolecules (polymers and proteins), and the chemical equilibria of molecular species.²⁷ Previous works demonstrated the accuracy of this method in studying the interaction between proteins and surfaces.^{12,28–30}

The first step in the theory is to write an approximate expression of the 3D semi-grand canonical potential, $\Omega(T, V, N_{\text{pol}}, \mu_j)$, where T is the temperature of the system, V is the volume, N_{pol} is the number of polymer chains grafted to the surface, and μ_j is the chemical potential of the mobile species (anions, cations, protons, and hydroxyls). Eqn (1) illustrates the different terms of the potential:

$$\beta\Omega = -S_{\text{trans}}/k_{\text{B}} - S_{\text{conf}}/k_{\text{B}} + \beta F_{\text{electr}} + \beta F_{\text{chem}}^{\text{pol}} + \beta F_{\text{chem}}^{\text{prot}} - \sum_j \beta N_j \mu_j, \quad (1)$$

where k_{B} is the Boltzmann's constant, and $\beta = 1/k_{\text{B}}T$.

The first term in eqn (1) represents the translational entropy of all mobile species (cations, anions, H^+ , and OH^-). The second term, S_{conf} , accounts for the conformational entropy of the end-tethered polymer chains. The third term, F_{electr} , captures the electrostatic interactions in the system. The terms $F_{\text{chem}}^{\text{pol}}$ and $F_{\text{chem}}^{\text{prot}}$ correspond to the enthalpic contributions from the acid–base equilibria of the polymer and the

protein, respectively, allowing us to explicitly consider the acid–base reactions of the titratable amino acids in the proteins and the monomers on the surface. Finally, the last term, $\beta N_j \mu_j$, represents the grand canonical contribution from all mobile species. In this description, the position and orientation of the protein is fixed, therefore we considered that the mobile species and the polymer chains can instantaneously adapt to the protein position. The explicit expressions for the different contributions in eqn (1) can be found in a previous publication from our group, in which we studied the translocation of different proteins through a modified nanopore with weak polyelectrolytes.²⁹

To solve the theory, we must first obtain the functional extreme of the semi-grand canonical function, $\beta\Omega$, with respect to several unknown variables: the density of all mobile species, $\rho_i(\mathbf{r})$; the charge distribution of amino acids and acidic segments of the polymer, expressed in terms of the degree of charge of amino acid j in the adsorbing protein $f_j^{\text{prot}}(\mathbf{r})$, and $f^{\text{pol}}(\mathbf{r})$, the degree of charge of the grafted polymer at position \mathbf{r} ; the electrostatic potential of the system, $\psi(\mathbf{r})$; and the probability of finding a given polymer chain j in conformation α , $P_j(\alpha)$. Due to the coupling of these expressions, an analytical solution is not possible, so we employed a Jacobian-free Newton method³¹ and discretized the system onto a 3D lattice. The input required to solve the theory includes the molecular and chemical details of the system, which are described in the following section. The output of the calculations comprises the molecular organization of the system (the local densities of all mobile species and the probability of the different conformations of the polymers), the electrostatic potential, the chemical state (protonated/deprotonated) of all titratable species (both in the grafted polymers and in the protein), and, importantly, the free energy of the system for a fixed position and orientation of the adsorbing protein. We refer the interested reader to ref. 29 for further details.

Molecular models

To solve the theory, we need to specify details regarding the surface (morphology, curvature, surface functionalization), the bath solution, the polymer, and the protein models.

In order to investigate the effect of curvature on the protein adsorption process, we studied a system consisting of either a planar surface or a spherical surface, a nanoparticle (NP), of different radii ($R_{\text{NP}} = 1, 3, 5, 7.5, 10$ nm, see Fig. 1A). In all cases, the surface was functionalized with polymers of 16 neutral segments per chain and a terminal titratable acidic segment, such that the surface density for all systems was comparable, 4.67–4.55 polymers per nm^2 , similar to reported values for Au-SAMs.³² Given the different geometry of the systems, this resulted in a calculation box size and different number of total polymers on the surface. These details can be found in Table S1 in the SI.

To model the polymers grafted to the surface, we considered a coarse grain scheme in which the polymer sequence consists of 16 neutral segments and one end-group acidic segment, similar to 16-mercaptohexadecanoic acid. The

volume for all the segments in the chains was set to 0.027 nm^3 , while the charge of the segments was 0 or -1 , corresponding to the neutral/protonated or the deprotonated group respectively. The acidic group has a $\text{p}K_{\text{a}} = 4.8$, that corresponds to the ideal monomer in solution. The speciation diagram of the monolayer that results from grafting the polymers to a planar surface can be found in Fig. S1 in the SI, and is discussed in the Results section. The dielectric constant of the polymer is set to 3.0 in order to represent the behavior of the neutral chains.¹¹ To describe the polymers grafted to the surface, we need to generate a representative set of conformations. For a proper representation of the chains, we used 100 000 randomly generated polymer conformations at each grafting position on the surface, created using a segment length of 0.153 nm (ref. 11) and the Rotational Isometric State (RIS).³³ Only conformations that do not overlap with the surface or the protein were considered. It is worth mentioning that the set of chain conformations is generated once for each geometry, and then used for all the corresponding calculations reported here.

The modified surface is in contact with a solution bath (Fig. 1A) for which we need to specify the salt concentration and pH bulk value. In our calculations, these quantities were typically fixed at 10 mM and 7, respectively, unless otherwise specified. The volume and charge of all mobile species is specified in Table S2 in the SI, and the relative dielectric constant of the solvent, was set to 78.54 everywhere in the system.

The protein structures were obtained from the Protein Data Bank (PDB). We employed distinct literature-reported structures for cytC in its oxidized and reduced states. Specifically, the structure of the oxidized cytC is PDB ID:1HRC,³⁴ and for the reduced cytC is PDB ID:1GIW.³⁵ These structures were selected because they represent the highest-resolution structures available for horse-heart cytochrome c in the oxidized and reduced states and are widely used as reference models in the literature.²⁰

In our calculations, the protein was treated as a rigid body, with all amino acid positions fixed relative to the center of mass of the protein. In this way, we did not take into account conformational changes upon protein adsorption onto the different surfaces. This approximation is generally valid between pH 4 and 9;¹³ outside this range, oxidized cytC undergoes conformational changes.²⁰ Furthermore, several spectroscopic studies report native-fold retention on carboxylated SAMs within this pH-range.^{20,36–38} To assess the impact of orientation on protein behavior, we performed 864 rotations of the protein at each position relative to the surface.

We employed a coarse-grained model to represent the protein, in which each amino acid is depicted as two solid beads: one for the backbone and one for the side chain, except for glycine, which is represented by a single backbone bead, similar to a previous work with the theory.¹² Depending on the nature of the amino acid, the side chain is either neutral or titratable. The equilibrium constants for all titratable amino acids are provided in Table S3 in the SI. We needed to coarse grain the heme group as well, for what we considered the iron

atom, the propionate, the pyrrole groups and the ethyl groups as different beads (see Fig. S2 in the SI), each with its own volume and charge (see Table S4).

Further details on the polymer and protein models can be found in the SI.

Results and discussion

In this work, we set out to study the interactions between the heme protein cytochrome *c* and polymer-modified surfaces of different curvature, focusing on how curvature, redox state, pH, and salt concentration influence the adsorption process, as illustrated in Fig. 1A. These surfaces are coated with a weak electrolyte brush, characterized by a surface density of 4.55–4.67 chains per nm². Polymer chains are uniformly distributed on the surface and consist of a block of 16 neutral segments, with a terminal titratable acidic segment. The system comprises a single cytC molecule at a fixed distance from the surface, immersed in a reservoir of solvent molecules (water) and ions (OH⁻, H⁺, cations, and anions). For each calculation, the pH and salt concentration of the bulk solution are specified as input parameters. The protein is modeled using a coarse-grained approach, as shown in Fig. 1B.

To gain a deeper understanding of the interactions driving the adsorption process, we examined the effects of various parameters of the system on the free energy. We investigated the impact of the cytC oxidation state, the pH and salt concentration of the bulk solution, and the effect of surface curvature. In all cases, we computed the free-energy landscapes as a function of the protein–surface distance, while also sampling 864 different protein orientations to identify the most favorable configuration at each position. We assumed that the timescales of protein translation and rotation are slower than the equilibration times of small ions and polymers in the system, as similarly done in previous applications of the theoretical framework on protein and nanoparticle translocation.^{29,39,40} Based on this assumption, it is valid to analyze the free energy of the system for a fixed position and orientation of the protein relative to the surface.

Cytochrome *c* adsorption on planar surfaces

Since the adsorption process of cytC onto self-assembled, negatively charged molecular films on planar surfaces has been extensively studied, both experimentally^{20,22} and through molecular simulations,^{23,41} we begin our analysis by focusing on this setup, as it provides a well-characterized reference to compare and validate our model and theoretical framework. We explore both oxidized and reduced cytC, comparing our results with reported data. We then study the impact of pH and salt concentration on the process.

Impact of the redox state on the preferential orientation upon adsorption

In Fig. 2A, we present the free energy of the system as a function of the distance between the center of mass of the protein and the surface, for both oxidized and reduced cytC (as a refer-



Fig. 2 (A) Free-energy landscapes for the oxidized (red) and reduced (blue) cytC as a function of the distance to the surface. The markers represent the average free energy of the system for all rotations, whereas the vertical lines span the free-energy range at each position. Lines connecting the symbols are a guide to the eye. The surface is modified by polymers with $N = 16$ neutral segments per chain with a terminal titratable acidic segment, and a surface density $\sigma_{\text{pol}} = 4.55$ chains per nm². In all cases, $\text{pH}_{\text{bulk}} = 7.0$ and salt concentration was set to 10 mM. The cartoons above depict the modeled system at different protein–surface distances. (B) Representation of the most favorable orientation at the distance of minimum free energy for each oxidation state. The heme group in each redox state of cytC is highlighted in red.

ence, we take the free energy of the protein in the bulk as zero). Each point represents the mean free energy across all sampled orientations, with vertical lines indicating the range of free-energy values resulting from the different rotations considered (*i.e.*, the range between the orientations with the lowest and highest free-energy values). In this case, and for all other cases, unless stated otherwise, the pH and salt concentration are set to 7.0 and 10 mM, respectively. We chose these conditions because experimental work with Au-NPs and cytC is usually carried out at similar neutral pH values and relatively low salt concentrations.²⁰

As can be seen in Fig. 2A, for the conditions under study, the free-energy curves display a minimum with an equilibrium distance of ~ 3.75 nm from the surface. This behavior derives from attractive electrostatic interactions between protein and surface brush, as we analyze below. Regarding oxidation state, the curves for oxidized and reduced cytC are very similar, both in the depth of the free-energy well and the position of the minimum. At large distances ($d > 10$ nm), the free energy gradually approaches a constant value due to the increasing separation between the protein and the surface.

Far from the surface, where the protein and the brush interact negligibly, the total energy approximates the sum of the isolated components. This non-interacting state is taken as the reference point for the zero free energy. When the protein gets closer to the surface, the electrostatic interactions between the protein and the acidic brush grafted to the surface become more significant, in a manner that depends on the charge state of the protein and the polymer brush, and therefore, the pH and the salt concentration of the bath solution.

For the pH under consideration (pH = 7) the polymer brush is partially ionized (*ca.* 25%), imparting a negative charge to the surface coating (see Fig. S1 in the SI). In contrast, the protein is positively charged, since the pH value is below the isoelectric point of cytochrome *c* (pI = 10.2–10.5,⁴² see Fig. S3 in the SI). This scenario leads to attractive electrostatic interactions that decrease the free energy of the system, as observed. However, when the protein is at distances shorter than the minimum ($d < 3.75$ nm), steric repulsions between the protein and the polymer brush become dominant, increasing the free energy of the system abruptly.

Regarding the impact of the protein orientation, we observe that it plays an increasingly significant role as the protein gets closer to the surface, and the electrostatic interactions between the protein and the polymers become stronger. This is evidenced by the vertical lines in the figure, which represent the range of free-energy values obtained for different protein orientations at a fixed distance from the surface. This broad distribution stems from the heterogeneity in the charge distribution of the protein, arising from the location and protonation states of its various titratable amino acids. Fig. 2B shows a schematic representation of the most favorable orientation at the position of minimum free energy for each oxidation state. Although the free-energy curves for oxidized and reduced cytC are very similar in terms of the average free energy across all orientations (represented by the central markers in Fig. 2A), we do observe important differences regarding the orientation that the protein acquires upon adsorption onto the surface, indicating that the most stable orientation strongly depends on its oxidation state. Interestingly, the lowest free-energy value among all orientations—corresponding to the bottom of the vertical bar in Fig. 2A—is lower for the oxidized form. This observation is consistent with previous computational results based on Molecular Mechanics/Generalized Born Surface Area (MM/GBSA) calculations.²³

To accurately describe the orientation of the protein at the surface, we define two rotational angles: α , the tilt angle of the

heme group, measured between the Fe–S_{Met80} bond and the vector normal to the surface (Z-axis); and ϕ , which considers the rotation of the heme around its own axis. A detailed explanation with a visual representation of these angles is provided in Fig. S4 in the SI. For both redox states, the most favorable orientation places the heme pocket facing the surface (Fig. 2B), consistent with a $\phi \approx 190^\circ$. However, the tilt angle of the heme differs significantly: in the oxidized state, the heme lies at $\alpha \approx 130^\circ$, while in the reduced state, it is nearly perpendicular to the surface, at $\alpha \approx 80^\circ$. Furthermore, while the oxidized form exhibits a well-defined minimum, the reduced cytC presents several orientations with similar free-energy values, suggesting that multiple configurations could be thermally accessible at room temperature. This is supported by the orientational energy landscapes (see top row of Fig. S5 in the SI), and aligns with previous molecular dynamics studies that reported comparable orientational flexibility.²³

To further validate our results, we compared the predicted surface proximity of lysine residues in the most stable orientation of oxidized cytC with experimental data from differential methylation assays.²² Lysines predicted to be closest to the surface matched those with decreased methylation reactivity upon adsorption, and *vice versa* for the more exposed residues (see Table S5 in the SI), supporting the accuracy of our orientational predictions. In addition, our results also indicate that electrostatic interactions and steric repulsions are sufficient to accurately describe the cytC adsorption onto the modified surface. Despite relying on a rigid-body approximation, our model successfully reproduces key features observed experimentally and in molecular dynamics simulations, including the preferred orientation, adsorption free energy, and residue-level accessibility patterns.

Finally, we analyzed the specific contribution of the iron redox state to the observed reorientation by performing additional calculations with hybrid models: the oxidized structure (1HRC) with ferrous heme iron and the reduced structure (1GIW) with ferric heme iron. As shown in the bottom row of Fig. S5 and in Fig. S6 in the SI, the preferred orientations and free-energy profiles of these hybrids closely match those of the original structures, indicating that the reorientation is not driven by the formal heme iron charge alone, but instead reflects subtle differences in surface charge distribution and local rearrangements around the heme pocket between the two experimental structures.

Impact of charge-regulation mechanisms and protein orientation on the adsorption process

In Fig. 2A we can see that around ~ 10 nm the free energy of the system begins to decrease as the protein becomes closer to the surface, as is to be expected when approaching opposite charges. As the protein gets closer, the electrostatic interactions between the protein and the surface become significant, modulated by the charge state of the protein and the polymer brush, the pH and the salt concentration of the bath solution.

We also observe that the charge of the protein changes as it approaches the surface, becoming more positively charged than in bulk solution, see Fig. 3A. As reflected in the figure, the redox state of the protein has little effect. Since both the protein and the monolayer contain titratable groups (amino acids or acidic segments, respectively), depending on the conditions of the solution, they can regulate their charge in order to optimize these electrostatic interactions. They would do so by shifting their acid–base equilibrium, at the expense of

chemical free energy. This charge regulation mechanism has been described for both protein^{12,28,29} and polymer brushes,^{10,43} and we want to deepen the analysis on its effect on protein adsorption for our studied system. At $\text{pH}_{\text{bulk}} = 7$, the surface monolayer is negatively charged, as shown in Fig. S7B (SI), promoting the protonation of the titratable amino acids in cytC, in a manner that depends on the orientation of the protein, since it determines the distance of each amino acid to the surface. This is reflected in the vertical lines for each point in Fig. 3, showing the dispersion of values for each protein rotation considered in the calculations. We can also observe this in Fig. 3B, where we plot the free energy of the system as a function of the charge of the adsorbed protein at the equilibrium distance (see Fig. 2). As shown in Fig. 3A, the protein increases its positive charge upon adsorption, enhancing electrostatic attraction with the negatively charged surface (see also Fig. S7A in the SI).

This becomes more pronounced around 5–6 nm from the surface, value that compares nicely to the Debye length for a planar charged surface in a 10 mM KCl solution (3.04 nm), adding the thickness of the surface monolayer ~ 2 nm (Fig. 6B, blue curve). The phenomenon of charge regulation has been described before for proteins in the proximity of charged surfaces¹² and proteins translocating through modified nanopores²⁹ and it is also what is taking place in this case, as the protein becomes closer to the surface. For the equilibrium distance from the surface, the protein is slightly more positively charged than in bulk ($\Delta Q_{\text{prot}} \sim 1.5$). Given the pH of the bulk solution (7.0) and the magnitude of the shift in charge, this is due to the acid–base equilibrium of the two histidine residues, given their pK_{a} is around 6.0 (see Table S3 in the SI). For distances closer to the surface, we see in Fig. 2 a steep increase in free energy that is mainly driven by strong steric repulsions. Further charge optimization would require the involvement of additional amino acids, but at a high energetic cost due to their pK_{a} mismatch with the $\text{pH}_{\text{bulk}} = 7.0$ (see Table S3 in the SI).

Charge regulation is also occurring in the surface monolayer, two-fold in this case. The first shift in the acid–base equilibrium of the terminal titratable acidic segment is due to the fact that the group is part of a polymer grafted to a surface, with a given surface density. This can be observed in Fig. S1 in the SI, where we see that the titration curve for the ideal acidic monomer in solution is shifted almost 3 units towards higher pH values for the surface monolayer (no protein). This shifts the apparent pK_{a} of the monolayer to ~ 7.8 , compared to 4.8 for the monomer in solution. For the monolayer, strong electrostatic repulsions between same charge head groups result in the system shifting the equilibrium towards the protonated (and neutral) state. The magnitude of this shift is related to the high surface density of the grafted polymer (4.55 chains per nm^2). Similar results have been observed for planar brushes.¹⁰ The second charge regulation mechanism comes into play when the protein approaches the surface (see Fig. S7 in the SI). In this case, depending on the pH of the bulk solution, the protein will bear a positive or a negative charge, that



Fig. 3 Analysis of protein charge regulation for a cytC molecule approaching a planar surface functionalized with polymers of 16 neutral segments per chain and a terminal titratable acidic segment. Surface density is $\sigma_{\text{pol}} = 4.55$ chains per nm^2 . In all cases, $\text{pH}_{\text{bulk}} = 7.0$ and salt concentration was set to 10 mM. (A) Change in the total charge of the protein with respect to its bulk value as a function of the distance to the surface. The markers represent the average of charge change for all rotations, whereas the vertical lines span the range of the change in protein charge at each position. Lines connecting the symbols are a guide to the eye. The gray vertical dashed line indicates the equilibrium distance equal to 3.75 nm (see Fig. 2A). (B) Free-energy values for the 864 different orientations of oxidized cytC at their equilibrium distance, as a function of the protein charge.

would in turn translate into attractive or repulsive interactions, respectively. Then, the surface monolayer would up-regulate or down-regulate the deprotonation of the acid group, depending on the pH of the bulk solution (Fig. S7 in the SI).

So far we have analyzed the charge of the protein as a whole entity, when in reality proteins have an anisotropic distribution of charges in space, making protein orientation a key aspect in several processes. Fig. 3B is a reflection of this fact, showing the free energy of the system as a function of the total charge for each rotation of the oxidized cytC at the equilibrium distance from the surface, where we see that there is no clear correlation between the total charge of the protein and the free energy (results for the reduced form of cytC can be found in Fig. S8B in the SI). This implies that a more positive net charge does not necessarily correlate with a stronger affinity for the negatively charged surface. To get a deeper look into this, it is essential to highlight that the net charge represents the sum of both positive and negative charges, underscoring the significance of the orientation of the positive charges relative to the surface.

To further explore the preference for different orientations relative to the charged surface, we examined the relationship between the free energy for each rotation and the dipole moment of the adsorbed protein (at the position of the minimum for the curve free energy *versus* distance, Fig. 2). This approach has been previously used to analyze the relative orientation of a protein inside a charge-modified nanopore, showing strong correlations and good descriptors.²⁹ Results for oxidized cytC are summarized in Fig. 4 (see results for the reduced cytC in Fig. S8 in the SI).

In Fig. 4A we see that for the adsorbed cytC, the most stable orientations correspond to the ones with the dipole moment vector pointing towards the charged surface, whereas the least stable orientations point away (the center of the protein is

marked with a green sphere). Each arrow points from the negative charges toward the positive charges. The spatial arrangement can be rationalized once again bearing in mind that for the considered pH_{bulk} of 7.0 the surface monolayer is negatively charged, with its charged groups arranged in a plane parallel to the surface, generating an electrostatic potential ψ (see Fig. 4B) in which the anisotropically charged protein orients itself in order to optimize electrostatic interactions. Given the symmetry of the system, there is no clear correlation between the free energy of the system and dipole moment of the adsorbed cytC molecule in the xy -plane (the plane of the surface monolayer, Fig. 4C). This can be appreciated in Fig. 4C and in the fact that the most stable orientations arrange themselves onto a cone directed towards the surface. On the other hand, as expected, the z -component of the dipole-moment has better correlation with respect to the relative free energy as it can be observed in Fig. 4D. For the reduced cytC adsorbed onto the modified surface we observe the same qualitative behavior (Fig. S8 in the SI), with the protein oriented preferably with its dipole moment point towards the surface. Even though the dipolar approximation may be too simplistic to represent a complex distribution of charges such as a protein, it still allows us to capture and interpret the main features governing the adsorption.

Effect of pH and salt concentration on the adsorption process

As mentioned so far, in our system, the interactions between the grafted polymer brush and the cytC molecule are primarily electrostatic in nature. In this context, it is to be expected that both the pH and the concentration of the supporting electrolyte play a key role in modulating the range of electrostatic interactions. Furthermore, both the acidic head groups in the polymer grafted to the surface and the titratable amino acids



Fig. 4 Analysis of protein orientation for an oxidized cytC molecule adsorbed onto a planar surface functionalized with polymers of 16 neutral segments per chain and a terminal titratable acidic segment. Surface density is $\sigma_{\text{pol}} = 4.55$ chains per nm^2 . In all cases, $\text{pH}_{\text{bulk}} = 7.0$ and bulk salt concentration is 10 mM. (A) Schematic representation of the surface in the (x,y) plane and the cytC molecule at the equilibrium distance (green circle). The blue and red arrows represent the vectors of the dipole moment for the ten conformations with the lowest and the highest free-energy values, respectively. (B) Colormap of the electrostatic potential at $\text{pH} = 7.0$. Polymer chains are included for illustration purposes only. Fig. 6B below shows that the extension of the polymer brush is ≈ 2.5 nm, in accordance with the computed electrostatic potential. (C) Free energy as a function of the dipole distance in the xy -plane, μ_{xy} , for all protein orientations considered at their equilibrium distance. (D) Free energy as a function of the dipole moment in the axial direction, μ_z , for all protein orientations considered at their equilibrium distance.

in the protein regulate their charge in a manner that depends on the pH and salt concentration of the bulk solution and the charge state of the groups.

We explored the free energy of the system for a molecule of oxidized cytC and the surface monolayer at bulk pH values between 3 and 11 and bulk salt concentration values of 10, 100, and 1000 mM. Given that oxidized and reduced cytC display similar average adsorption free energies and charge regulation profiles, and that more experimental data are available for the oxidized form,²⁰ we focus the following analysis on the oxidized form of cytC. In our model we do not take into account conformational changes that the cytC molecule may undergo under extreme pH conditions, such as the acid-induced unfolding (below pH \sim 4) and the alkaline transition (above pH \sim 9), both of which have been extensively characterized.²⁰ Nevertheless, analyzing these pH regimes using a rigid-body approximation allows us to isolate and quantify the electrostatic contribution to adsorption, even in the absence of pH-induced structural changes.

First we analyze the effect of bulk pH for a fixed salt concentration of 10 mM. Fig. 5A shows the mean free energy of the system as a function of the distance from the surface for different bulk pH values (4.0, 7.0, and 11.0). All curves display a minimum, indicating protein adsorption, with the distance corresponding to the free-energy minimum remaining nearly unchanged by pH, while the depth varies significantly, in a non-monotonic manner. The strongest adsorption is observed for $\text{pH}_{\text{bulk}} = 7.0$, while increasing or decreasing the pH makes protein-surface interaction less favorable. This can be rationalized again taking into consideration the charge state of all species in the different conditions, and how the pK_{a} of the surface monolayer (\sim 7.8) compares to the pI of the protein (\sim 10).

At $\text{pH}_{\text{bulk}} = 4.0$, when the protein is sufficiently away from the surface (\sim 10 nm), the monolayer is almost uncharged, given most of the acidic groups would be protonated (Fig. S7B

in the SI), while the protein is highly positively charged (Fig. S3 in the SI). However, when the protein comes closer, it induces a small ionization of the acidic groups in the polymer chains (\sim 10%), and once again electrostatic interactions are established, resulting in the free-energy minimum observed in Fig. 5. It is worth noting that even if the dissociation fraction is only \sim 10%, this still yields a considerable negative surface charge due to the high grafting density ($\sigma_{\text{pol}} = 4.55$ chains per nm^2), leading to an adsorption free energy of \sim -15 $k_{\text{B}}T$.

Increasing bulk pH to 7.0 leads to a deeper free-energy minimum. In that pH range (4.0–7.0), the acidic groups in the polymer chains begin to deprotonate, up to \sim 30% (Fig. S7B in the SI). Even though protein charge becomes less positive (Fig. S3 in the SI), still the increase in negative charge on the surface is enough to increase the free energy of adsorption to \sim -30 $k_{\text{B}}T$.

For $\text{pH}_{\text{bulk}} = 11.0$, we still observe a free-energy minimum at around 3.75 nm from the surface, but we also observe a slight barrier between 5–10 nm. At that pH, the polymer brush is almost fully deprotonated and strongly negatively charged (Fig. S7B in the SI), while the protein is slightly above its isoelectric point ($\text{pI} \sim$ 10), bearing also a total negative charge. This leads to electrostatic repulsions that translate into the barrier we observe between 5–10 nm. Now, when the protein becomes closer to the surface, it is also able to regulate its charge to a certain degree, as explained above. For the pH under consideration, our calculations show that around 5 nm there is a charge inversion in the protein net charge, from negative to positive (Fig. S7A in the SI), shifting from electrostatic repulsions (barrier) to attractions (minimum). This is due to the fact that $\text{pH}_{\text{bulk}} = 11.0$ is quite close to cytC pI (\sim 10, Fig. S3 in the SI), making this pH range very sensitive to charge regulation mechanisms in the protein.

Regarding the effect of bulk salt concentration, in Fig. 5B we show how the free energy as a function of the distance to the surface changes for ionic strength values of 10, 100 and

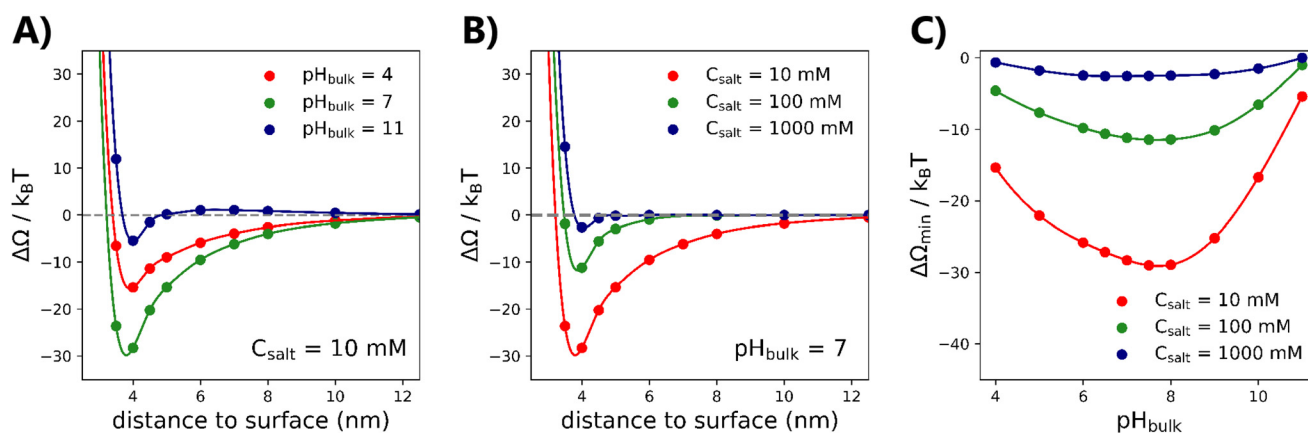


Fig. 5 Analysis of pH and salt concentration effect on the adsorption process of oxidized cytC onto a planar surface functionalized with polymers of 16 neutral segments per chain and a terminal titratable acidic segment. Surface density is $\sigma_{\text{pol}} = 4.55$ chains per nm^2 . (A) Free-energy curves as a function of the distance of cytC to the surface for different values of pH_{bulk} , as indicated in the figure. $C_{\text{salt}} = 10$ mM. The markers represent the average free energy of the system for all rotations. For clarity, we omit the vertical bars spanning the free-energy range at each position. (B) Free-energy curves for different bulk salt concentration, as indicated in the figure. $\text{pH}_{\text{bulk}} = 7.0$. (C) Mean free energy of adsorption for cytC adsorbing onto planar surface system as a function of bulk pH for different bulk salt concentration, as indicated in the legend.

1000 mM, for a fixed pH_{bulk} of 7.0. Here again we observe that all curves display a free-energy minimum, with its position remaining nearly unchanged by salt concentration, while the depth varies greatly. As the salt concentration increases, the free energy of the system decreases significantly due to the supporting electrolyte effectively screening the electrostatic interaction between the protein and the surface, reducing the attractive coulombic forces between them at this pH. At a supporting electrolyte concentration of 1 M, even though a minimum is observed, the free energy of interaction is in the order of $k_{\text{B}}T$, suggesting that cytC is unlikely to be electrostatically adsorbed under these conditions. This has also already been described experimentally.⁴⁴

Fig. 5C summarizes the change of the free energy as a function of pH for different salt concentrations, computed at a fixed protein–surface distance corresponding to the position of the free-energy minimum observed in panels A and B. We observe that for each salt concentration considered, the free energy of adsorption as a function of pH displays a minimum around $\text{pH}_{\text{bulk}} = 8$. This minimum becomes smoother as the concentration of salt increases, almost disappearing for $c_{\text{salt}} = 1$ M, following the increase in electrostatic screening as the supporting electrolyte concentration goes up. The position of the minimum around 8 can be rationalized considering how the pH of the solution compares to the pK_{a} of the monolayer (~ 7.8) and the pI of the protein (~ 10). At pH values below ~ 8 , the acidic group in the polymer chains begin to protonate, becoming fully protonated around $\text{pH} \sim 4$, which results in a near-zero surface charge density (see Fig. S1 and S7B in the SI), while the protein acquires a highly positive net charge. Conversely, at pH values greater than the minimum, the

polymer brush is nearly fully deprotonated, while the protein approaches its isoelectric point (pH 10), leading to a lower total charge close to zero. In both cases, the attractive interactions decrease due to the proximity of neutrality in one of the components.

Cytochrome *c* adsorption onto curved surfaces

In the previous sections, we explored the adsorption of cytC onto planar surfaces under different conditions, identifying key parameters governing the adsorption process. Here we extend our study by taking into account the effect of the surface curvature, particularly for spherical nanoparticles (NPs) of various sizes (NP radius $R_{\text{NP}} = 1, 3, 5, 7.5, 10$ nm). Given that we did not observe a great impact of the redox state of the heme group in the behavior of the cytC adsorption onto planar surfaces, in what follows, we focus only on the oxidized state at pH 7 and a salt concentration of 10 mM.

Fig. 6A shows the free energy of the system at different protein–surface distances for NPs with radii 1 nm and 5 nm and the limiting case of a planar surface. Similar to the planar case at the same pH and salt concentration, for all NP sizes considered, the free-energy curves exhibit a strongly repulsive behavior at short range, mainly due to steric repulsions, a minimum well at intermediate range, and at long range, the attraction weakens and the free energy approaches zero. As discussed above, this is due to the charge state of the surface monolayer and the protein at the given pH and ionic strengths conditions. We observe a gradual shift in the position of the minimum (adsorption distance) and a steeper repulsive branch as the curvature decreases. Both behaviors can be rationalized taking into account how the available volume

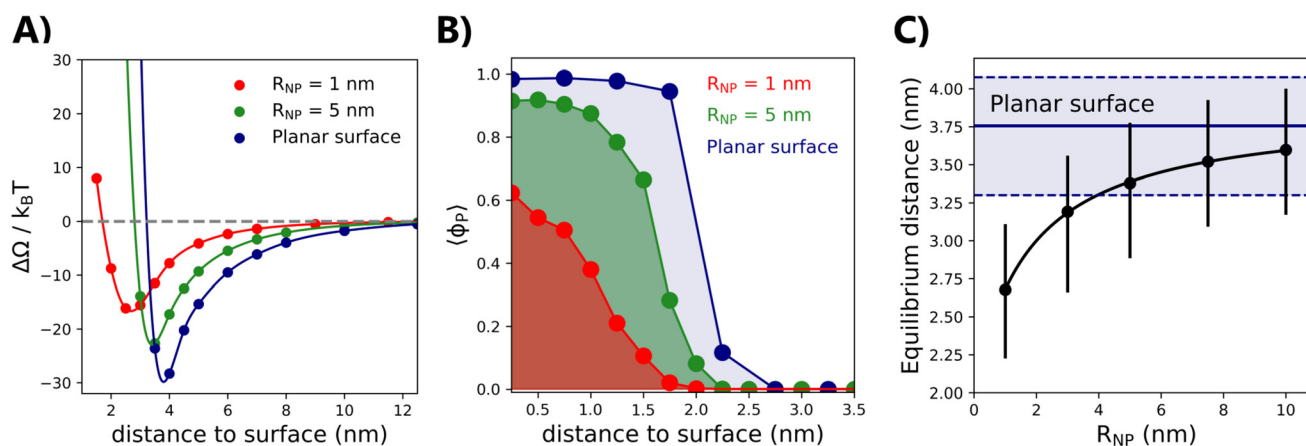


Fig. 6 Analysis of curvature effect on the adsorption process of an oxidized cytC molecule onto spherical NPs of different radii modified with polymers of 16 neutral segments per chain and a terminal titratable acidic segment. Surface density is $\sigma_{\text{pol}} = 4.67$ chains per nm^2 (4.55 chains per nm^2 for the planar surface). In all cases, $\text{pH}_{\text{bulk}} = 7.0$ and salt concentration was set to 10 mM. (A) Free energy as a function of the distance of oxidized cytochrome *c* to the surface of NPs of different radii. The markers represent the average free energy of the system for all rotations. For clarity, we omit the vertical bars spanning the free-energy range at each position. (B) Average volume fraction occupied by the polymer ($\langle \phi_{\text{p}} \rangle$) as a function of the surface distance for different radius of curvature. (C) Position of the minimum of the free-energy curves for nanoparticles of different radii. The marker represents the mean distance within all rotations, whereas the vertical lines span the range of distances for each NP radius. The solid blue line represents the average distance between all orientations for the case of a planar surface, whereas the region between the dashed blue lines spans the different equilibrium distances adopted for each orientation.

changes as we move away (or closer) to convex surfaces of different sizes. For curved convex surfaces, the available volume increases as we move away from the surface, scaling with $(r/R)^3$ for spheres (where r is the radial distance to the surface and R is the radius of the surface). Increasing the size of the NP decreases the available volume at a given distance from the surface, and this in turn increases the polymer-polymer steric repulsions within the monolayer. Moreover, same charge deprotonated acidic groups repel one another, so decreasing available volume also implies increasing repulsive forces between them. This translates into a more stretched polymer layer towards the solution. As seen in Fig. 6B, as the radius increases, the polymer chain expands to a longer range. On highly curved surfaces, the relative volume available as the chain moves away from the surface increases more abruptly compared to planar surfaces. With more free space available, the chains can adopt more constrained dispositions, gaining conformational freedom and, on average, arranging themselves closer to the surface. In contrast, on planar surfaces, the conformational freedom is highly hindered due to packing constraints. Consequently, the polymer brush extends further from the surface. This affects directly the adsorption distance of cytC onto NPs of different sizes, as can be seen in Fig. 6C. We observe that this distance monotonically increases towards the expected value for a planar surface, with a change in adsorption distance of up to 36% as compared to the 1 nm NP. We realize this size is very small from an experimental point of view, but our results could be relevant for nanomaterials of different shapes, such as Au nanostars, which can display spikes of sizes ~ 1 nm, that would affect electronic transfer processes.²⁵

Surface curvature also has a significant impact on protein adsorption, primarily through its effect on charge regulation mechanisms. Fig. 7 shows how both the net charge of the protein (panel A) and the dissociation fraction of the acidic groups in the polymer brush (panel B) vary as a function of distance to the surface for nanoparticles of different radii.

As discussed for the planar case above, the distance to the surface is a key factor modulating charge regulation. Two observations are immediately apparent: first, as previously discussed for the planar case, we observe that at the pH considered ($\text{pH}_{\text{bulk}} = 7.0$), shorter distances to the surface promote protonation of titratable amino acids in cytC, driven by the negative charge of the surface monolayer. This leads to an increase in the overall protein charge (see Fig. 6A and 7A). The second observation is that for a fixed distance to the surface, calculations show that the protein charge difference increases as the NP becomes larger, implying that the charge regulation mechanism in place becomes more significant as the radius increases, recovering the behavior observed for planar surfaces when $R_{\text{NP}} \rightarrow \infty$ (planar surface). This is also evident in Fig. S9 in the SI, where we show how the protein charge differs with respect to the protein in the bulk, plotted as a function of the radius of the NP, for two different distances of the center of mass of the protein and the surface, 3.5 and 7 nm. These observations reflect the presence of two com-

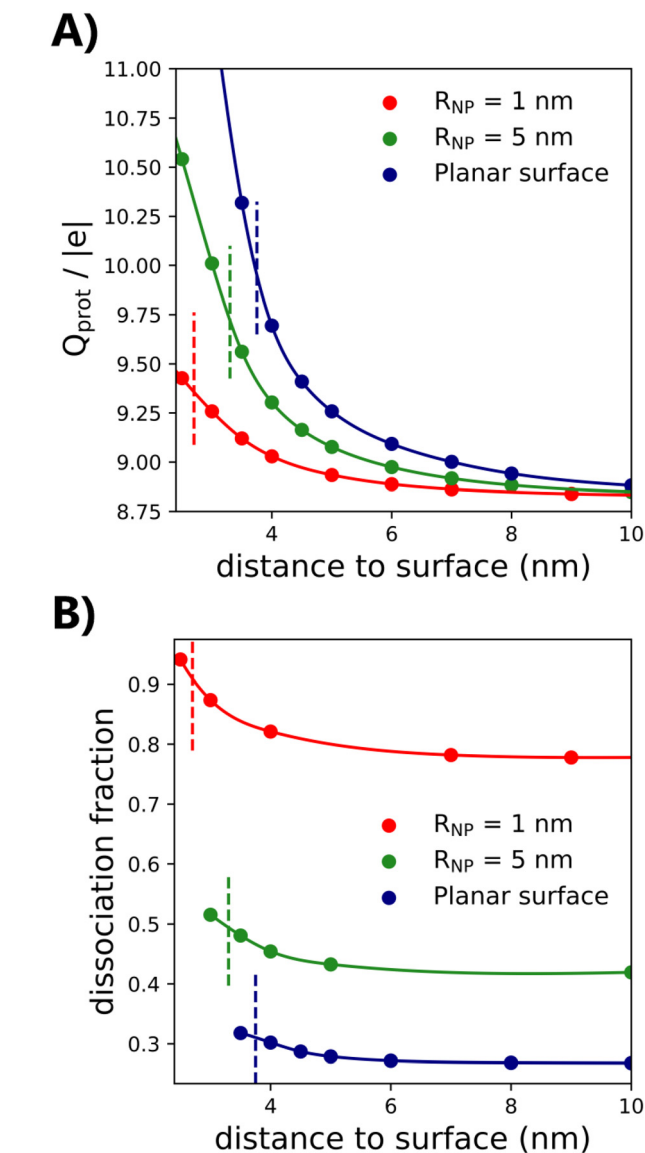


Fig. 7 Analysis of charge regulation for the adsorption of oxidized cytC onto NPs of variable radii functionalized with polymers of 16 neutral segments per chain and a terminal titratable acidic segment. Surface density is $\sigma_{\text{pol}} = 4.67$ chains per nm^2 (4.55 nm^{-2} for the planar surface). The results corresponding to the planar surface are also displayed. In all cases, bulk pH values and c_{salt} are kept fixed at 7.0 and 10 mM, respectively. (A) Oxidized cytC net charge as a function of the distance to the surface. (B) Dissociation fraction of the acidic head groups of the polymer brush for different protein distances and nanoparticle radii. Only the polymers under the projected area of the protein are taken into account for the calculation. In both panels, the vertical dashed lines indicate the equilibrium distance in each case, *i.e.* 2.7 nm, 3.3 nm and 3.75 nm for $R_{\text{NP}} = 1$ nm, $R_{\text{NP}} = 5$ nm and the planar surface, respectively.

peting effects. On one hand, as shown in Fig. 6B, a larger radius causes the polymer chains to extend towards the solution, thus reducing the distance between the negatively charged surface monolayer and the protein. This in turn translates into a greater degree of charge regulation on both sides: the protein and the acidic end-group of the grafted chains (see Fig. 7A).

Moreover, while the polymer chain density was fixed and kept constant for all NPs ($\sigma_{\text{pol}} = 4.67$ chains per nm^2), an increase in NP radius results in a greater number of polymer chains on the surface. This leads to more charged groups interacting with the protein, further promoting amino acid protonation (Fig. 7A). On the other hand, smaller radii enhance the dissociation of the ionizable acid–base groups anchored to the chains.¹¹ Our calculations show that the dissociation fraction on the 1 nm NPs (~ 0.8) almost doubles that on the 5 nm NP (~ 0.45) and triples that of the planar system (~ 0.25) (Fig. 7B). This means that the surface monolayer will down-regulate its charge as the NP becomes larger, with the limiting value being that of the planar surface (discussed above). In this way, decreasing NP size while keeping the bulk pH constant, will result in a larger negative surface charge density. However, since surfaces with low curvature exhibit a greater protein charge difference (Fig. 7A and S9), we infer that the increase in negative charge due to greater dissociation has a smaller impact compared to the combined effects of chain proximity and density discussed above.

Finally, we analyzed the effect of curvature on the orientation of the adsorbed protein onto NPs of different sizes. As we can see in Fig. 8A, both rotational angles, α (the tilt angle of the heme group) and ϕ (the rotation of the heme around its axis), change significantly with NP radius, reaching the limiting value of planar surfaces for NP radius ~ 10 nm. In Fig. 8B we see the most favorable orientation for the adsorbed cytC molecule at a planar surface compared to a NP with $R_{\text{NP}} = 1$ nm. We observe there is a critical NP size for which there is a sharp change in both angles ~ 7 – 8 nm. We attribute this change in orientation with NP size with the change in interactions given the geometry of the system. To deepen the analysis, we computed the dipole moment of the most stable orientations of the protein adsorbed onto NPs of different sizes, and we observed that the change in protein orientation is accompanied by a change in the direction of the dipole moment with respect to the normal to the surface, described by the angle θ (Fig. S10A in the SI). At small radii (< 5 – 7 nm), the dipole vectors represent molecular orientations closely aligned with the local surface normal ($\theta \sim 180$ – 170°). Upon increasing the radius, tangential contributions grow, and the orientations progressively splay outward, resembling the shape of a widening cone (Fig. S10B in the SI). We interpret this tilting to increasing lateral interactions, as the surface is commensurate with the size of the protein: cytC has an approximate size of ~ 2 – 3 nm,⁴⁵ and the surface monolayer has a thickness of ~ 2 – 2.5 nm, depending on the NP size (Fig. 6C). This means that for NP = 1 nm, considering the surface polymers, the total size is similar to that of the protein, and not much lateral interactions can occur. However, this changes as the NP increases in size, translating into more spread lateral protein orientations.

These curvature-dependent changes in protein orientation and interfacial charge regulation are likely to impact electron transfer processes, given the strong sensitivity of electronic

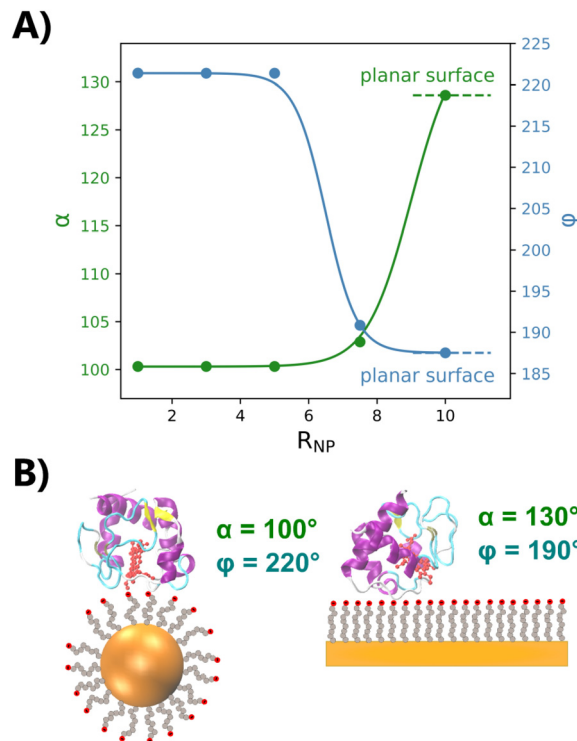


Fig. 8 (A) Analysis of the most favorable orientation of oxidized cytC adsorbed onto nanoparticles' surfaces of different radii. The orientation for each radius is determined by α (in green) and ϕ (in light blue). The lines connecting the symbols are a guide to the eye. α and ϕ corresponding to the planar surface is also displayed with dashed lines. (B) Representation of the most favorable orientation at the distance of minimum free energy of oxidized cytC for a planar surface and a nanoparticle of radius of 1 nm. The heme group of cytC is highlighted in red. The α and ϕ angle in each case is explicated. In all cases, $\text{pH}_{\text{bulk}} = 7.0$ and salt concentration was set to 10 mM.

coupling to both distance and the relative alignment of redox-active sites with respect to the surface.⁴⁶

Conclusions

In this study, we thoroughly investigated the interactions between cytC and surfaces modified with carboxylated polymers, analyzing the effect of the redox state of the protein, the pH and salt concentration of the solution, and the curvature of the surface, comparing planar surfaces with spherical NPs of different sizes. We employed a molecular theory that explicitly accounts for the size, shape, conformations, and charge of all molecular species within the system. This approach also incorporates the acid–base equilibria of the titratable amino acids in the protein and of the carboxylic end-group in the grafted polymers on the surface. By performing 3D calculations, we were able to comprehensively investigate the influence of protein orientation, explicitly considering multiple rotational configurations. Our results showed that considering electrostatic and steric interactions was enough to capture the nature of the adsorption process, successfully reproducing key fea-

tures observed experimentally and in molecular dynamics simulations, including the preferred orientation, adsorption free energy, and residue-level accessibility patterns. Electrostatic interactions between the charged amino acids of the protein and the surface-grafted polymers result in attractive energy profiles, characterized by a minimum whose position and depth depend strongly on the pH and salt concentration of the solution, the orientation of the protein relative to the surface, and the surface curvature. Our calculations revealed that the difference between oxidized and reduced cytC has a greater effect on the preferred orientation of the protein than on the overall adsorption free-energy profile, indicating that the most stable orientation is highly sensitive to the oxidation state of the protein.

We also investigated the role of charge regulation mechanisms in protein adsorption, showing that the overall charge of the protein becomes more positive as it approaches the surface, while the carboxylic groups in the surface monolayer increase their degree of deprotonation. This chemical communication during the adsorption process is highly dependent on the interplay between the isoelectric point of the protein, the pK_a of the monolayer, the pH of the solution, and its ionic strength. By modulating pH and salt concentration, cytC can be adsorbed or desorbed from the surface.

Due to the anisotropic distribution of charges within the protein, its orientation relative to the surface also plays a key role in the adsorption process. Using the dipole moment of the protein as a proxy for this local charge distribution, our calculations revealed that the most stable orientations tend to align along a cone directed toward the surface.

Finally, surface curvature has a significant influence on protein adsorption by affecting both the molecular organization of the system and the charge regulation mechanisms at play. As nanoparticles become larger, the polymer brush extends further into solution, increasing the equilibrium distance between the protein and the surface, while simultaneously rotating the heme edge of cytC. For cytC, these curvature-driven shifts in distance and orientation are not merely structural, as heterogeneous ET rates depend exponentially on separation and sensitively on orbital alignment. The calculated trends therefore provide a mechanistic link to the enhanced ET activity reported for curved gold nanostructures and offer concrete design rules for nanoparticle electrodes and catalytic platforms that exploit cytochrome-based redox chemistry.

Future work will extend the present molecular theory framework to proteins whose adsorption is dominated by hydrophobic or dispersion forces, or whose net dipole is weak, to test whether curvature controlled steric confinement can still direct orientation in the absence of strong electrostatics.

Author contributions

Conceptualization: S. M. Z., E. G. S., M. A. C., Y. A. P. S.; formal analysis: S. M. Z.; funding acquisition: Y. A. P. S., M. A. C., E. G. S.; investigation: S. M. Z.; methodology: S. M. Z., E. G. S.,

M. A. C., Y. A. P. S.; resources: Y. A. P. S., E. G. S.; software: S. M. Z., Y. A. P. S., E. G. S.; validation: S. M. Z., E. G. S., Y. A. P. S.; visualization: S. M. Z.; writing – original draft: S. M. Z., E. G. S., M. A. C., Y. A. P. S.; writing – review & editing: S. M. Z., E. G. S., M. A. C., Y. A. P. S.

Conflicts of interest

There are no conflicts to declare.

Data availability

Data for this article are available at Softmatter-FCEN at <https://github.com/softmatter-FCEN>.

The code for the program implemented to solve the molecular theory equations can be found at https://github.com/mario-taglia/crystal/tree/PDB_NP.

Supplementary information: Molecular models and details, definition of the rotational angles α and ϕ , analysis of surface distances of lysine residues in oxidized cytC adsorbed on a planar surface, free-energy maps of the adsorption of cytC onto a planar surface for different protein orientations, charge regulation for the adsorption of oxidized cytC onto a planar surface, analysis of protein orientation for reduced cytC adsorbed onto a planar surface, impact of curvature on protein charge regulation and orientation. See DOI: <https://doi.org/10.1039/d5nr02326b>.

Acknowledgements

E. G. S., M. A. C. and Y. A. P. S. are fellows of CONICET. S. M. Z. is a doctoral CONICET fellow. This research was funded by grants PICT-2020-SERIEA-00188, PICT-2020-SERIEA-00176, PICT-2021-I-INVI-00491 (ANPCyT), PIBAA 2022-2023 28720210100765CO (CONICET), UBACYT 20020220400215BA (UBA).

References

- 1 P. Gomez-Romero, A. Pokhriyal, D. Rueda-García, L. N. Bengoa and R. M. González-Gil, *Chem. Mater.*, 2024, **36**, 8–27.
- 2 D. Zhang, Y. Chen, M. Hao and Y. Xia, *Angew. Chem., Int. Ed.*, 2024, **63**, e202319567.
- 3 S. A. Bhakta, E. Evans, T. E. Benavidez and C. D. Garcia, *Anal. Chim. Acta*, 2015, **872**, 7–25.
- 4 A. Stern, A. P. Petersen, H. C. Zierden and G. A. Duncan, *Cell Biomater.*, 2025, **1**, 100043.
- 5 J. M. Bolivar, J. M. Woodley and R. Fernandez-Lafuente, *Chem. Soc. Rev.*, 2022, **51**, 6251–6290.
- 6 F. Borzouee, J. Varshosaz, R. A. Cohan, D. Norouzian and R. T. Pirposhteh, *Curr. Med. Chem.*, 2021, **28**, 3980–4003.

- 7 A. B. Asha, Y. Chen and R. Narain, *Chem. Soc. Rev.*, 2021, **50**, 11668–11683.
- 8 H. J. Tanudjaja, A. Anantharaman, A. Q. Q. Ng, Y. Ma, M. B. Tanis-Kanbur, A. L. Zydney and J. W. Chew, *J. Water Process. Eng.*, 2022, **50**, 103294.
- 9 Z. Xi, R. Zhang, F. Kiessling, T. Lammers and R. M. Pallares, *ACS Biomater. Sci. Eng.*, 2024, **10**, 38–50.
- 10 R. Nap, P. Gong and I. Szleifer, *J. Polym. Sci., Part B: Polym. Phys.*, 2006, **44**, 2638–2662.
- 11 D. Wang, R. J. Nap, I. Lagzi, B. Kowalczyk, S. Han, B. A. Grzybowski and I. Szleifer, *J. Am. Chem. Soc.*, 2011, **133**, 2192–2197.
- 12 F. M. Boubeta, G. J. Soler-Illia and M. Tagliacuzzi, *Langmuir*, 2018, **34**, 15727–15738.
- 13 J. Meissner, Y. Wu, J. Jestin, W. A. Shelton, G. H. Findenegg and B. Bharti, *Soft Matter*, 2019, **15**, 350–354.
- 14 G. Yu and J. Zhou, *Phys. Chem. Chem. Phys.*, 2016, **18**, 23500–23507.
- 15 I. Fenoglio, S. Gul, F. Barbero, E. Mecarelli, C. Medana, A. Gallo and C. Polizzi, *Heliyon*, 2024, **10**, e40587.
- 16 S. Yang, C. Peng, J. Liu, H. Yu, Z. Xu, Y. Xie and J. Zhou, *Biointerphases*, 2024, **19**, 051005.
- 17 C. Zhang, X. Li, Z. Wang, X. Huang, Z. Ge and B. Hu, *J. Phys. Chem. B*, 2019, **124**, 684–694.
- 18 F. Tavanti, A. Pedone, P. Matteini and M. C. Menziani, *J. Phys. Chem. B*, 2017, **121**, 9532–9540.
- 19 D. Mohammadyani, V. E. Kagan and J. Klein-Seetharaman, *Biophys. J.*, 2013, **104**, 503a–504a.
- 20 D. Alvarez-Paggi, L. Hannibal, M. A. Castro, S. Oviedo-Rouco, V. Demicheli, V. Tórtora, F. Tomasina, R. Radi and D. H. Murgida, *Chem. Rev.*, 2017, **117**, 13382–13460.
- 21 S.-i. Imabayashi, T. Mita and T. Kakiuchi, *Langmuir*, 2005, **21**, 2474–2479.
- 22 J. Xu and E. F. Bowden, *J. Am. Chem. Soc.*, 2006, **128**, 6813–6822.
- 23 D. Alvarez-Paggi, D. F. Martín, P. M. DeBiase, P. Hildebrandt, M. A. Martí and D. H. Murgida, *J. Am. Chem. Soc.*, 2010, **132**, 5769–5778.
- 24 H. B. Gray and J. R. Winkler, *Annu. Rev. Biochem.*, 1996, **65**, 537–561.
- 25 C. M. Silveira, R. Zumpano, M. Moreira, M. P. de Almeida, M. J. Oliveira, M. Bento, C. Montez, I. Paixão, R. Franco, E. Pereira, *et al.*, *ChemElectroChem*, 2019, **6**, 4696–4703.
- 26 H. M. Berman, J. Westbrook, Z. Feng, G. Gilliland, T. N. Bhat, H. Weissig, I. N. Shindyalov and P. E. Bourne, *Nucleic Acids Res.*, 2000, **28**, 235–242.
- 27 G. Zaldivar, Y. A. Perez Sirkin, G. Debais, M. Fiora, L. L. Missoni, E. Gonzalez Solveyra and M. Tagliacuzzi, *ACS Omega*, 2022, **7**, 38109–38121.
- 28 E. Gonzalez Solveyra, D. H. Thompson and I. Szleifer, *Polymers*, 2022, **14**, 739.
- 29 E. Gonzalez Solveyra, Y. A. Perez Sirkin, M. Tagliacuzzi and I. Szleifer, *ACS Nano*, 2024, **18**, 10427–10438.
- 30 M. Cathcarth, A. S. Picco, G. B. Mondo, M. B. Cardoso and G. S. Longo, *J. Phys.: Condens. Matter*, 2022, **34**, 364001.
- 31 A. C. Hindmarsh, P. N. Brown, K. E. Grant, S. L. Lee, R. Serban, D. E. Shumaker and C. S. Woodward, *ACM Trans. Math. Softw.*, 2005, **31**, 363–396.
- 32 J. C. Love, L. A. Estroff, J. K. Kriebel, R. G. Nuzzo and G. M. Whitesides, *Chem. Rev.*, 2005, **105**, 1103–1170.
- 33 P. J. Flory, *Statistical Mechanics of Chain molecules*, Oxford University Press, New York, 1989.
- 34 G. W. Bushnell, G. V. Louie and G. D. Brayer, *J. Mol. Biol.*, 1990, **214**, 585–595.
- 35 L. Banci, I. Bertini, J. G. Huber, G. A. Spyroulias and P. Turano, *JBIC, J. Biol. Inorg. Chem.*, 1999, **4**, 21–31.
- 36 D. H. Murgida and P. Hildebrandt, *J. Phys. Chem. B*, 2001, **105**, 1578–1586.
- 37 D. H. Murgida and P. Hildebrandt, *Acc. Chem. Res.*, 2004, **37**, 854–861.
- 38 A. Sivanesan, H. K. Ly, J. Kozuch, M. Sezer, U. Kuhlmann, A. Fischer and I. M. Weidinger, *Chem. Commun.*, 2011, **47**, 3553–3555.
- 39 M. Tagliacuzzi, K. Huang and I. Szleifer, *J. Condens. Matter Phys.*, 2018, **30**, 274006.
- 40 Y. A. Perez Sirkin, M. Tagliacuzzi and I. Szleifer, *Soft Matter*, 2021, **17**, 2791–2802.
- 41 J. Zhou, J. Zheng and S. Jiang, *J. Phys. Chem. B*, 2004, **108**, 17418–17424.
- 42 L. Hannibal, F. Tomasina, D. A. Capdevila, V. Demicheli, V. Tortora, D. Alvarez-Paggi, R. Jemmerson, D. H. Murgida and R. Radi, *Biochemistry*, 2016, **55**, 407–428.
- 43 R. J. Nap, M. Tagliacuzzi, E. Gonzalez Solveyra, C.-l. Ren, M. J. Uline and I. Szleifer, in *Modeling of Chemical Equilibria in Polymer and Polyelectrolyte Brushes*, John Wiley & Sons, Ltd, 2018, ch. 6, pp. 161–221.
- 44 H. K. Ly, M. A. Marti, D. F. Martin, D. Alvarez-Paggi, W. Meister, A. Kranich, I. M. Weidinger, P. Hildebrandt and D. H. Murgida, *ChemPhysChem*, 2010, **11**, 1225–1235.
- 45 S. Akiyama, S. Takahashi, T. Kimura, K. Ishimori, I. Morishima, Y. Nishikawa and T. Fujisawa, *Proc. Natl. Acad. Sci. U. S. A.*, 2002, **99**, 1329–1334.
- 46 D. Zhao, L. Li and J. Zhou, *Appl. Surf. Sci.*, 2018, **428**, 825–834.